# The influence of projectile impact velocity and target characteristics on the terminal ballistics parameters of small-caliber projectile

#### Faris Memić<sup>1\*</sup>, Alan Ćatović<sup>2</sup>

- <sup>1</sup> Defense Technologies Department, Mechanical Engineering Faculty, University of Sarajevo, Bosnia and Herzegovina
- <sup>2</sup> Defense Technologies Department, Mechanical Engineering Faculty, University of Sarajevo, Bosnia and Herzegovina

\*Corresponding author E-mail: <a href="mailto:farismemic04@gmail.com">farismemic04@gmail.com</a>

Received: Jun. 5, 2024 Revised: Jul. 18, 2024 Accepted: Jul. 20, 2024

Online: Jul. 25, 2024

#### Abstract

The study examines the results of numerical simulations of the penetration of a 7,62 mm x 63, AP, M2 projectile through a target. Model validation involved a numerical simulation of 7,62mm x 63, AP, M2 projectile penetration through an AA5083H116 target, for which experimental results were available in the literature. The results of the numerical simulation were used for regression analysis - to calibrate the Recht-Ipson model for the given projectile. Furthermore, penetration analyses of 7,62 mm x 63, AP, M2 projectiles through various target materials were performed at consistent projectile velocities and mesh sizes. As expected, bainitic steels exhibited the highest resilience, demonstrating that increased material hardness and tensile strength correlate with enhanced projectile penetration resistance.

© The Author 2024. Published by ARDA.

*Keywords*: numerical simulation, penetration, 7,62mm x 63, AP, M2, Ansys, Autodyn

#### 1. Introduction

Projectile penetration through a target is a highly significant research topic for applications in defense technologies (i.e. ref [32]). Research on projectile penetration is crucial for understanding the fundamental mechanisms of protection against projectile impacts and armor design, as well as for enhancing the effectiveness of munitions against specific types of targets. There are three methods for analyzing projectile penetration: experimental, analytical, and numerical simulation methods. The experimental method is the most reliable, but it is also the most expensive and time-consuming. A drawback of the experimental method is that the results cannot be extrapolated to different ranges of variables beyond those used in the tests.

The analytical method can be used to perform certain analyses that yield usable results, such as the Recht-Ipson method. However, due to the complexity of modern systems, the analytical method is primarily used to gain insight into the nature of the penetration process. It can also be employed prior to conducting experiments; for example, a preliminary analytical approach can be used to establish a starting point and reduce the total number of experiments needed. Parametric analytical analysis is useful if the appropriate constants for the given target material and projectile type are known.



The numerical simulation method, which will be used in this study, has the capability to handle very complex geometries without any difficulties. Depending on the complexity of the material models used, results can range from the accuracy level of analytical models to that of experimental models. By setting up an adequate material model, any penetration simulation can be conducted seamlessly, yielding reliable results. Parameters such as impact velocity, target thickness, and impact angle (3D simulation is required for impact angle) can be varied as desired. Given the current advancements in hardware and software, numerical simulations can be conducted very quickly and at a much lower cost than experimental methods, while still providing high-accuracy results (provided the conditions for good accuracy are met, as outlined below). Accuracy depends on many parameters: the accuracy of the material model and constants in the models, the numerical model (mesh, solver, initial and boundary conditions), the type of simulation software used, etc.

# 2. Data on 7.62mm x 63, AP, M2 ammunition (USA: .30, AP, M2) and the weapons used with this type of ammunition

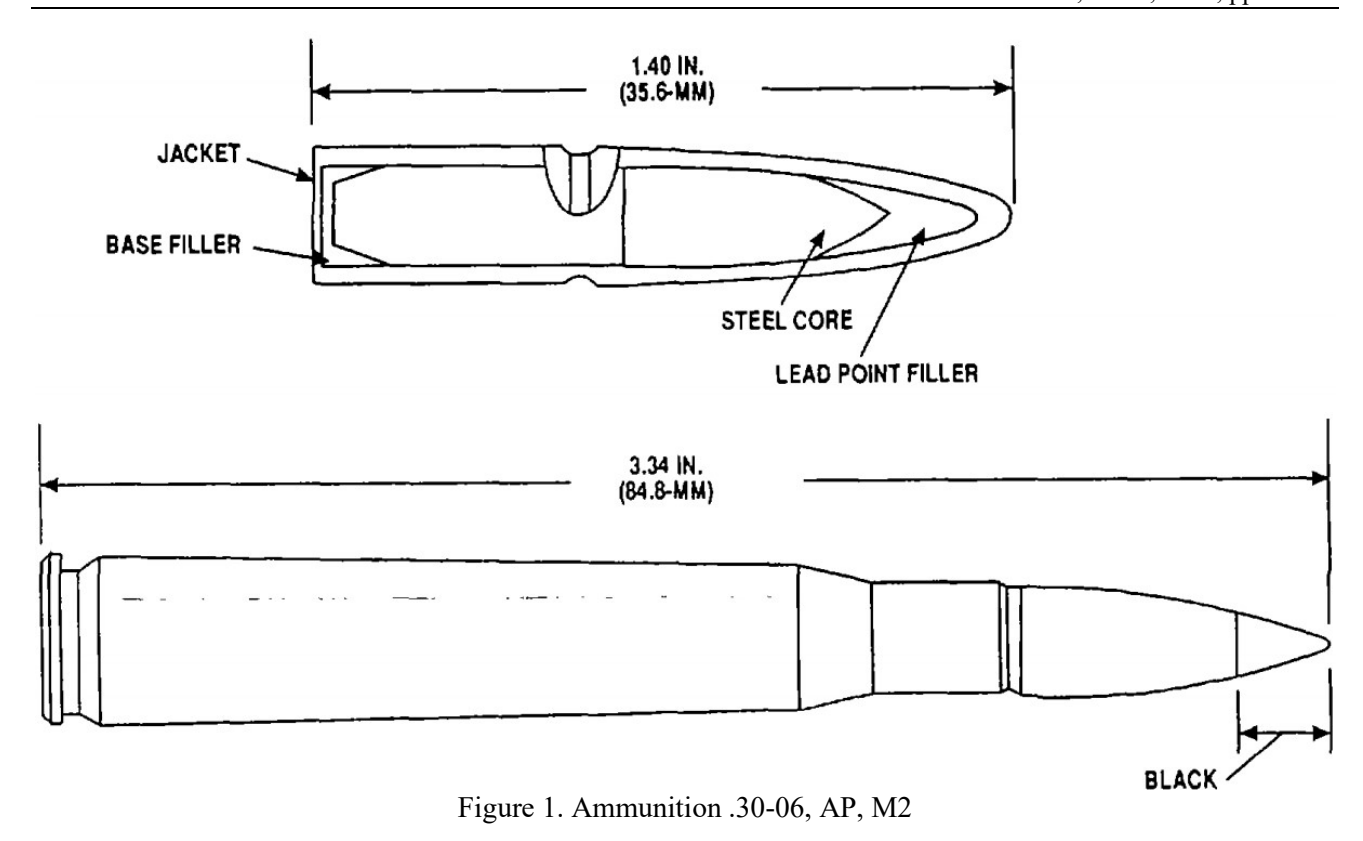
The American .30-06 AP, M2 / 7.62 mm x 63 ammunition was introduced in 1906 as an evolution of the US Army's short-lived use of the .30-03 cartridge, which was originally adopted in 1903 with a round-nosed bullet. The .30-06 cartridge has a slightly different case than the .30-03 and, more importantly, features an ogive-shaped projectile, providing significantly better aerodynamic performance. The 7.62 mm x 63 AP, M2 ammunition has a projectile mass of 10.8 grams, a muzzle velocity of 830 m/s, and a muzzle energy of 3730 J [1]. This ammunition is used against lightly armored vehicles, protective shelters, and infantry [2]. The basic data on this ammunition is provided in Table 1.

, , ,
1305-A202
Cartridges for weapons, inert projectile
27,5
84,8 mm
Impact
WC 852
3,6
10,8
ormance
372
827,5; at 23,8 m from muzzle
nd Storage Data
1.4S
Class V
С

Table 1. The basic data on ammunition .30-06, AP, M2 [3]

Figure 1 shows the 7.62mm x 63 (.30-06) AP, M2 ammunition and its cross-section. In the cross-section, the components of the ammunition can be seen: the brass jacket and case, the lead cap, and the steel core. The tip of the projectile is painted black to indicate armor-piercing ammunition.

Ammunition 7.62mm x 63, AP, M2 is fired from 7.62 mm machine guns, models: M37, M1919A4 and M1919A6, and a .30 caliber rifle, M1 [3]. In military service, the 30-06 was used in the bolt-action M1903 Springfield rifle, the bolt-action M1917 Enfield rifle, the semi-automatic M1 Garand rifle, the semi-automatic M1941 Johnson rifle, the Famage Mauser, the Browning Automatic Rifle (BAR), and numerous machine guns, including the M1917and M1919 series [4].



#### 3. Numerical simulations

# 3.1. Basics of the Autodyn software

The ANSYS Workbench platform enables interaction with ANSYS solvers. ANSYS Workbench is composed of different modules, eg: Explicit Dynamics, Meshing, Autodyn, etc. In ANSYS solvers, the terms "implicit" and "explicit" refer to two types of time integration methods used to perform dynamic simulations. Explicit time integration is more stable, but the simulation takes longer due to the small time-step (due to the high velocities, fine mesh, and high velocity of sound that are used in the materials) and is more efficient for simulations involving [5]:

- spreading of the shock wave,
- large deformations and stretching,
- non-linear behavior of material,
- complex contact between certain components
- fragmentation of material, etc.

Explicit methods calculate the state of the system in the next step based on the current state of the system, while implicit methods try to arrive at a solution by solving an equation involving the current state and the state of the system in the next step. Implicit methods require more computer resources and are much more difficult to implement. Compared to explicit, implicit methods have better stability, so larger time steps can be used with them. However, implicit methods require solving a large system of coupled equations for each time step, which significantly complicates the problem [5].

A typical application of the explicit dynamics module includes i.e. [5]:

- simulation of an object falling from a height
- impact and penetration process
- fragmentation
- explosions, etc.

The AUTODYN programs are general-purpose engineering software packages that use finite difference, finite volume, and finite element techniques to solve a wide variety of non-linear problems in solid, fluid, and gas dynamics. AUTODYN has a wide range of uses, eg: street explosions, building explosions, mine explosions, improvised explosive devices (IEDs), mining explosions, warhead design (cumulative charges), missile/warhead impact, aircraft impact, body armor, drop tests, destruction, etc. AUTODYN can be characterized as "many codes in one", and includes both structural mechanics and fluid mechanics regimes. Each of these "codes" in AUTODYN represents a specific numerical solver, for example [6]:

- Lagrange processor for modeling solid continua and structures
- Euler processors for modeling fluids, gases, and large distortion. These processors include first-order and second-order accurate schemes.
- ALE (Arbitrary Lagrange Euler) processor for specialized flow models
- Shell processor for modeling thin structural elements
- SPH (Smooth Particle Hydrodynamics).

Compared to the Eulerian approach, discussed below, the Lagrange formulation tends to be faster computationally as no transport of material through the mesh needs to be calculated. Moreover, material interfaces, free surfaces, and history-dependent material behavior are generally easier to follow in the Lagrange framework. The major disadvantage of Lagrange is that if excessive material movement occurs, the numerical mesh may become highly distorted leading to an inaccurate and inefficient solution. Further, this may ultimately lead to a termination of the calculation [6]. The calculations performed at each incremental time step (or cycle) in the Lagrange solver are shown schematically in Figure 2.

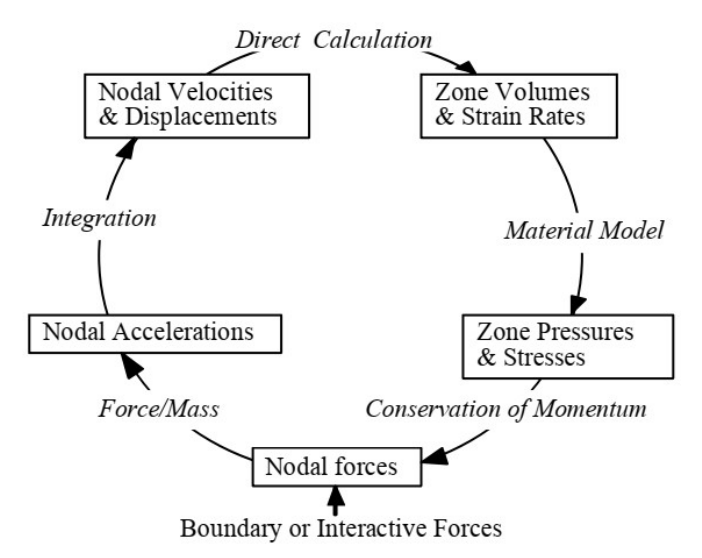


Figure 2. Lagrange Computation Cycle [6,31]

AUTODYN utilizes the differential equations governing unsteady material dynamic motion to express the local conservation of mass, momentum, and energy. In order to obtain a complete solution, in addition to appropriate initial and boundary conditions, it is necessary to define a further relation between The flow variables. The relations between the hydrostatic pressure, the local density (or specific volume), and the local specific energy (or temperature) are known as an equation of state [6].

The Rankine-Hugoniot equations for the shock jump conditions can be regarded as defining a relation between any pair of the variables  $\rho$ , p, e, u<sub>p</sub>, and U. Here, U is the velocity of the shock wave in the material, and u<sub>p</sub> is the velocity of the particles of the material. In many dynamic experiments making measurements of up and U, it has been found that for most solids and many liquids over a wide range of pressure, there is an empirical linear relationship between these two variables, viz. [6]:

$$U = c_0 + su_p \tag{1}$$

where  $c_0$  is the speed of sound, and s is an empirically determined constant.

AUTODYN uses the Mie-Gruneisen form of the equation of state, based on the so-called Hugoniot shock (an empirical curve showing the dependence of  $U(u_p)$ ,  $P(u_p)$ , or P(V), in the form [6]:

$$p = p_H + \Gamma \rho (e - e_H) \tag{2}$$

where  $\Gamma$  is the Gruneisen constant (for most materials it has a value of 1.25 ± 0.75). Also applies:

$$p_H = \frac{\rho_0 c_0^2 \mu (1 + \mu)}{[1 - (s - 1)\mu]^2}$$
(3)

$$e_H = \frac{1}{2} \frac{p_H}{\rho_0} \left[ \frac{\mu}{1+\mu} \right] \tag{4}$$

The Johnson-Cook model is a constitutive model that aims to model the strength behavior of materials subjected to large strains, high strain rates, and high temperatures. Such behavior might arise in problems of intense impulsive loading due to high-velocity impact and explosive detonation. The model defines the yield stress  $\sigma_y$  as [6]:

$$\sigma_Y = \left[ A + B \varepsilon_p^{\ n} \right] \left[ 1 + C \log \dot{\varepsilon_p} \right] \left[ 1 - T_H^{\ m} \right] \tag{5}$$

where:

 $\varepsilon_p$  – effective plastic strain,  $\varepsilon_p$  – normalized effective plastic strain rate (the ratio of the current strain rate to the reference strain rate  $\varepsilon_0$ ),  $T_H$  – homologous temperature  $(T-T_{room})/(T_{melr}-T_{room})$ . The five material constants are A, B, C, n, and m.

Johnson-Cook failure model is also an empirical model based on the tests with several metallic materials. It implements the effects of temperature softening and strain rate hardening. The basic form of the model, using the damage accumulation, can be seen in Equation [7]:

$$D = \sum \frac{\Delta \varepsilon}{\varepsilon_f} \tag{6}$$

where:

D – damage,  $\Delta \varepsilon$  - Increment of equivalent plastic strain during 1 integration cycle,  $\varepsilon_f$  - failure strain

Failure strain is defined as follows:

$$\varepsilon_f = [D_1 + D_2 e^{(D_3 \sigma^*)}] [1 + D_4 \ln \dot{\varepsilon}_p] [1 + D_5 T_H]$$
(7)

where

 $D_1$ - $D_5$  – material constants,  $\sigma^*$  - the ratio of stress to equivalent stress,  $\dot{\varepsilon}_p$  - normalized rate of plastic deformation,  $T_H$  - homologous temperature.

When D in Equation (7) becomes unity, failure occurs and the element is removed (eroded) from the computational grid [7].

Although AUTODYN can calculate with both Lagrangian and Eulerian subgrids it may sometimes be the case that materials have to be defined on Lagrangian subgrids even though it is clear that these materials will be subjected to very large distortions arising from the gross motion of the Lagrange grid [6].

During the subsequent calculation some of these Lagrangian cells can become grossly distorted and, unless some remedial action is taken, can seriously impair the progress of the calculation. Therefore, procedures have been incorporated into AUTODYN (both 2-D and 3-D) to remove such Lagrangian cells from the calculation if a pre-defined strain (either instantaneous geometric strain, incremental geometric strain, or effective plastic strain) exceeds a specified limit. When a cell is removed from the calculation process in this way the mass

within the cell can either be discarded or distributed to the corner nodes of the cell. If the mass is retained, conservation of inertia and spatial continuity of inertia are maintained. However, the compressive strength and internal energy of the material within the cell are lost whether or not the mass is retained. This discard procedure is known as erosion [6].

#### 3.2. The numerical model validation

Validation of the numerical model was performed using available experimental data (T. Borvik [8]) - from which data on the dimensions and material of the target, and the material of the projectile parts were also collected. A target of dimensions 150 mm x 150 mm and thickness 20 mm, AA5083H116, was used, for which experimental data are available in [8].

The target and the 7.62mm x 63 projectile were first modeled in the "SolidWorks" software (Figure 3) and then exported as a .iges file for insertion into the Ansys Workbench Explicit Dynamics module (Figure 4). A 2D model, axial symmetry, was used in the calculation, which was made on the basis of a 1/4 3D model in SolidWorks and using options in Geometry Modeler.

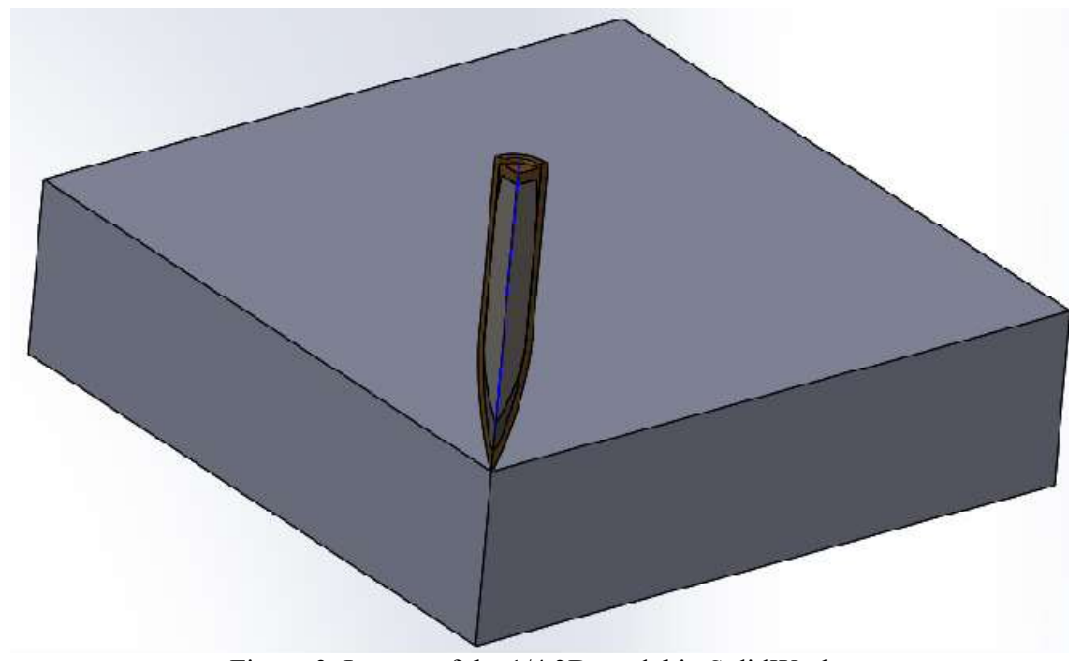


Figure 3. Layout of the 1/4 3D model in SolidWorks

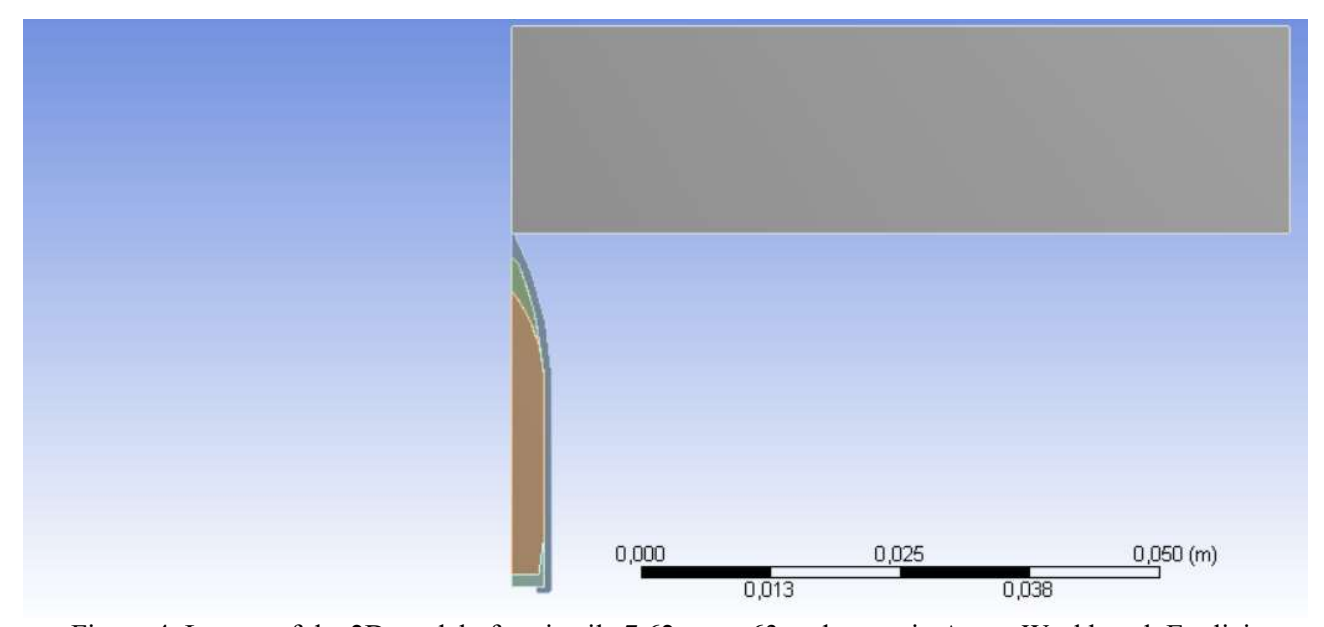


Figure 4. Layout of the 2D model of projectile 7,62mm x 63 and target in Ansys Workbench Explicit Dynamics module

In order to perform a sensitivity analysis of the numerical model grid, a 2D axisymmetric model with several different grids was discretized using the Lagrange solver (Figure 5). A comparison of the results was made for the following grids (mech element size): 0.1; 0.15; 0.2; 0.25; 0.3; 0.35; 0.4; 0.45 and 0.5 mm. The mesh was the same size for both the projectile elements and the target.

The condition of impact velocity in the y-axis direction (in the direction of penetration of the projectile through the target) of 822.4 m/s was set as stated in the reference [8]. Also, the target is fixed on the outer edge parallel to the axis of symmetry.

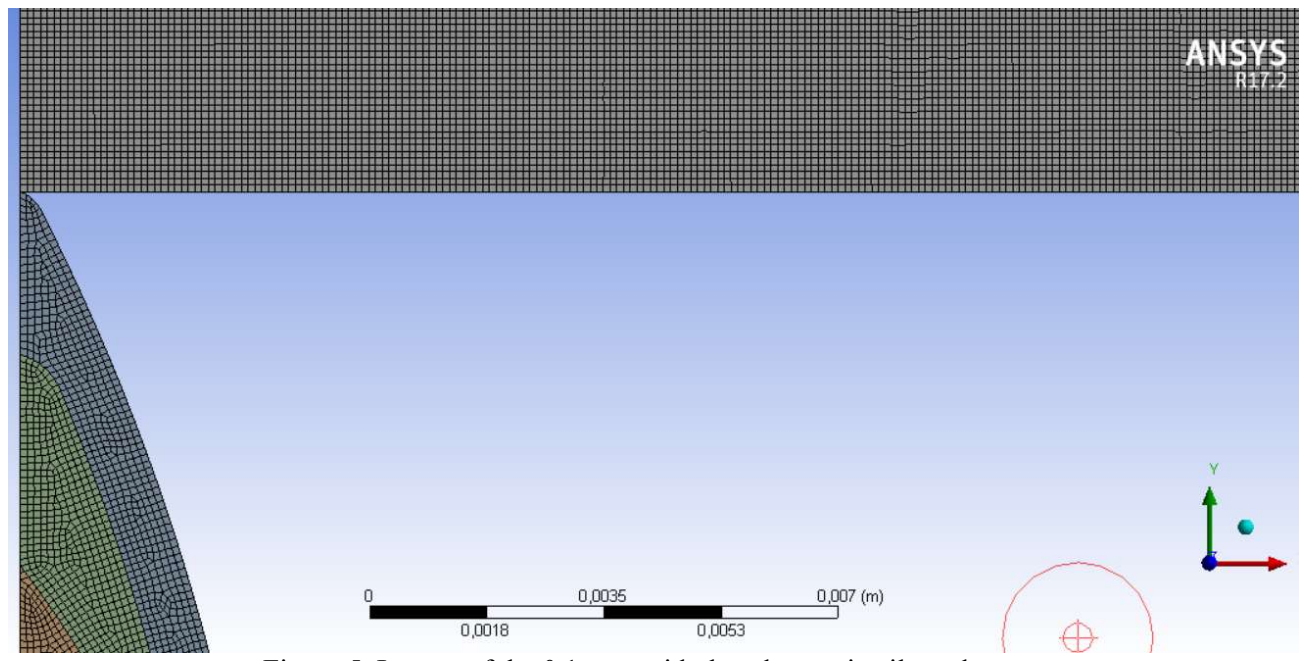


Figure 5. Layout of the 0,1 mm grid placed to projectile and target

Projectile material models (jacket, cup, core, and lead filling) were collected from the Ansys Autodyn library and combined with additional literature data [8]. The material models for the target were taken from the Ansys Autodyn library in combination with additional data from the literature [9].

For the plate that was used as a target (aluminum alloy AA5083H116), the Gruneisen shock equation of state with the following constants was used:  $\Gamma$ =1,97;  $\rho$ =2700 kg/m³;  $c_0$ =5340 m/s and s=1,4. Also, the Johnson-Cook model (strength model) was used, with the following constants: A=167 MPa; B=596 MPa; n=0,551; C=0,001 and m=0,859. The material failure model (Johnson-Cook) was also used on the target, with the following constants:  $D_1$ =0,0261;  $D_2$ =0,263;  $D_3$ =-0,349;  $D_4$ =0,147;  $D_5$ =16,8.

The projectile is composed of a steel core, a brass jacket and cup, and a lead tip. No failure model was used for the projectile parts. The Johnson-Cook strength model was used, the constants of the model are given in Table 2, as well as other material properties in Table 3.

Material	A (MPa)	B (MPa)	n	С	$\epsilon_0$ * (1/s)	m	$T_{m}\left(K\right)$
Steel (core)	1200	50000	1	0	0,0005	1	1800
Lead (tip)	24	300	1	0,1	0,0005	1	760
Brass (jacket and cup)	206	505	0,42	0,01	0,0005	1,68	1189

Table 2. Johnson-Cook constants for materials of projectile parts

Material	Density (kg/m³)	Young's modulus (MPa)	Poisson's ratio	Bulk modulus (Pa)	Shear modulus (Pa)	Specific heat capacity (J/kgK)
Steel (core)	7850	210000	0,33	2,0588·1011	7,8947·10 <sup>10</sup>	452
Lead (tip)	10660	1000	0,42	$2,0833\cdot10^9$	$3,5211\cdot10^{8}$	124
Brass (jacket and cup)	8520	115000	0,31	1,0088·1011	4,3893·10 <sup>10</sup>	385

Table 3. The main mechanical characteristics of the materials of projectile parts

In the reference [8], the initial velocity ( $v_i$  = 822.4 m/s) and the experimentally obtained exit velocity ( $v_r$  = 694.3 m/s) are given for the penetration test of the AA5083-H116 target material. The results of exit velocities obtained by numerical simulations as part of this validation are compared with the given projectile exit velocity obtained in the test. The relevant exit velocity is taken from the projectile element at the bottom of the projectile core because these elements are mostly used in the literature.

Exit velocities in the period from 90 to 100  $\mu$ s for different grids from 0.1 to 0.5 mm were analyzed. Because the values of the obtained exit velocities fluctuate around some mean value, the mean values of the velocity for a given bottom element and for each grid, in the time period from 90 to 100  $\mu$ s (when the projectile leaves the target), were calculated.

Figure 6 shows a diagram showing that the exit velocity settles at around 705.8 m/s, and considering that the 0.1 mm mesh has approximately the same velocity value, the 0.2 mm mesh gives sufficiently accurate simulation results. Also, the numerical simulation itself with a mesh of 0.2 mm takes much less time compared to a mesh of 0.1 mm. By comparing the exit velocity obtained by numerical simulation for a 0.2 mm mesh with the exit velocity obtained by the test in the literature [8], a relative error of 1.65% is obtained, which is a satisfactory result. Considering the small relative error, the 0.2 mm grid seems satisfactory and is adopted for further analysis in the paper.

The appearance of the penetration process of AP 7.62mm x 63 projectile at a time-frame of 50  $\mu$ s in the Ansys Workbench Explicit Dynamics module is shown in Figure 7, and in Figure 8 at a time-frame of 100  $\mu$ s. Qualitatively, the penetration simulation process is shown to resemble the penetration process presented also in the paper [8].

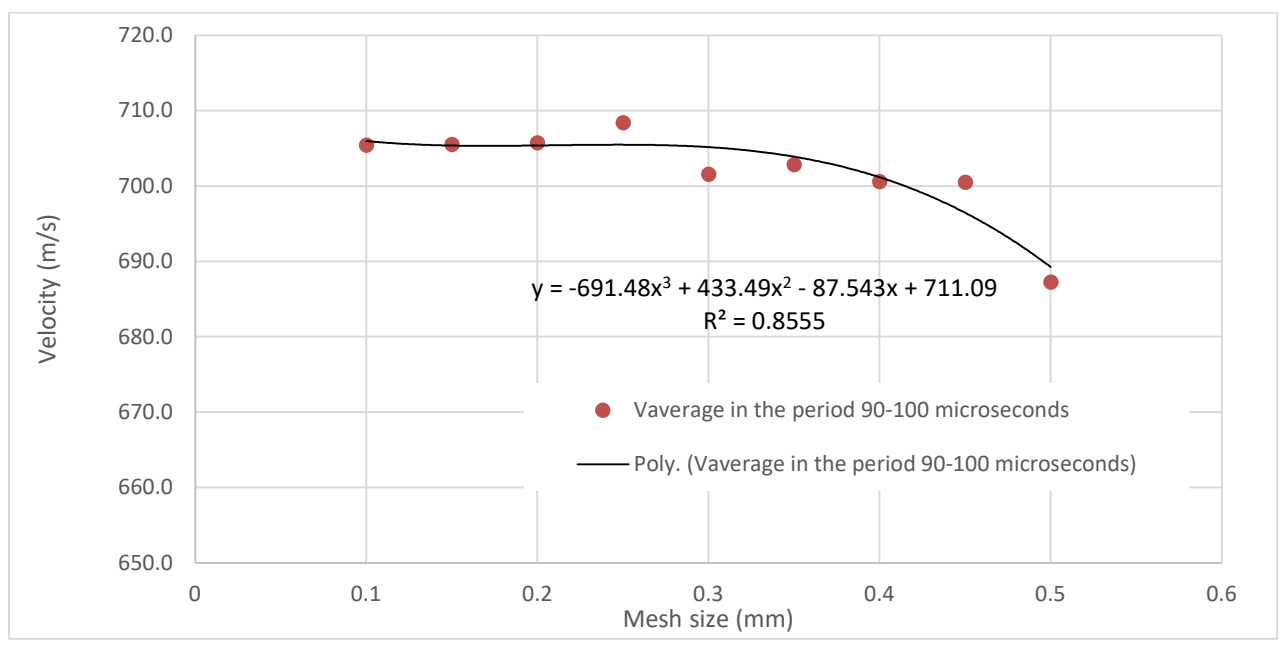


Figure 6. Display of the relationship between projectile exit velocity and mesh size and polynomial regression curve

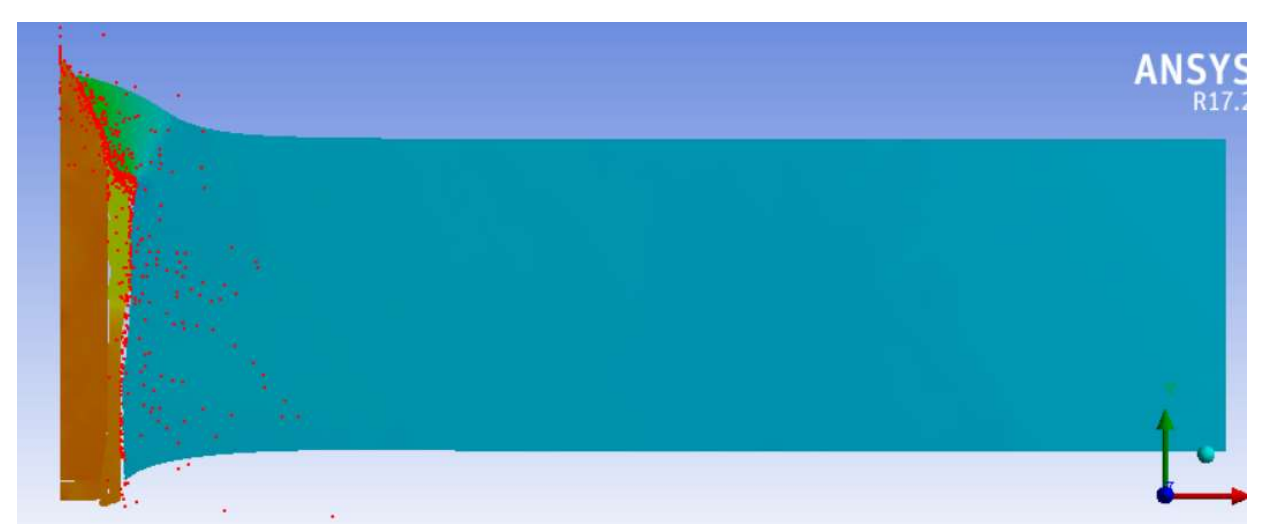


Figure 7. Display of the numerical simulation of the penetration of a 7.62mm x 63 caliber projectile through a target at the moment when the projectile is in the target

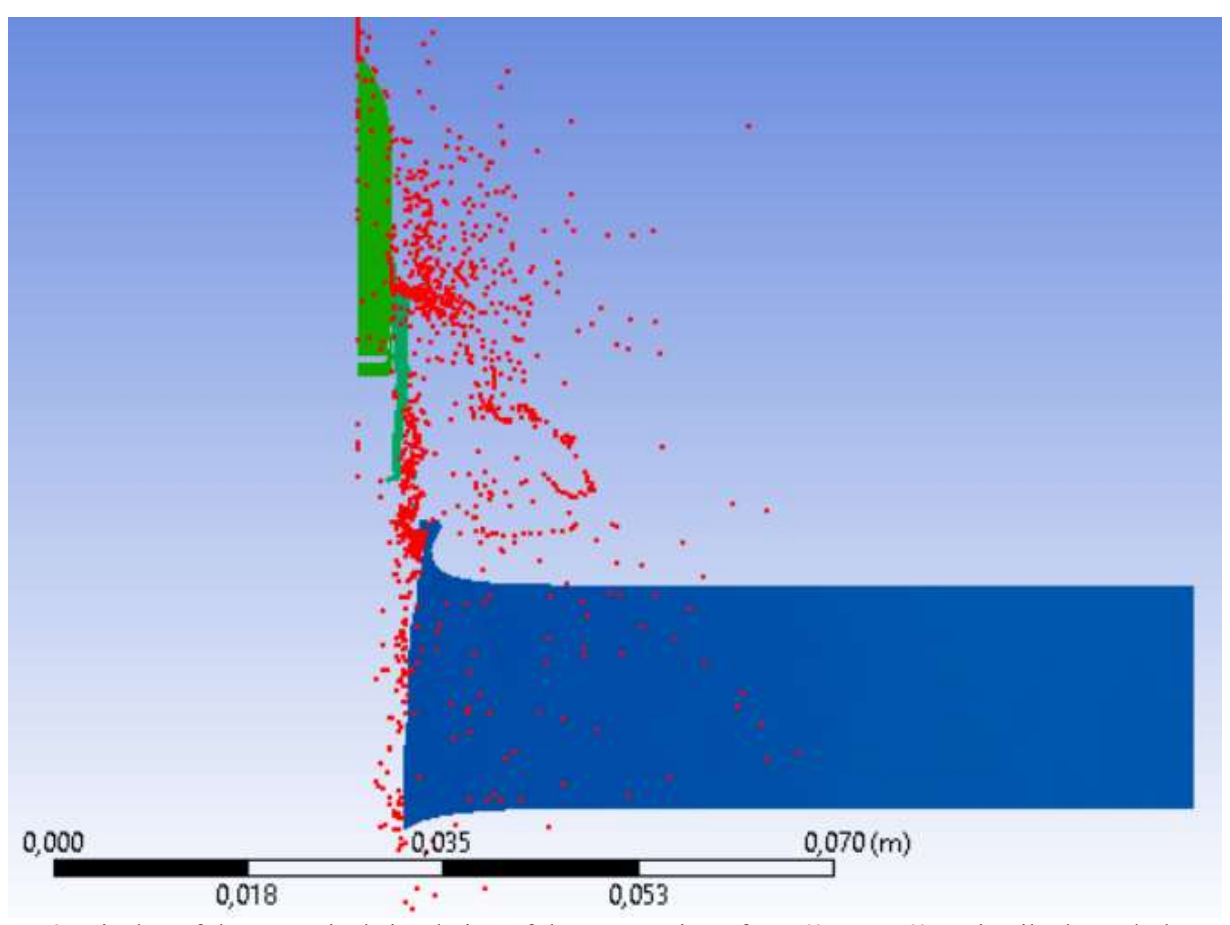


Figure 8. Display of the numerical simulation of the penetration of a 7.62mm x 63 projectile through the target at the moment when the projectile passed through the target

Figure 7. and Figure 8. shows that the core of the 7.62mm x 63 projectile remained almost undamaged during the penetration of the target. This is also recored in ref. [8] that served in validation process.

#### 3.3. Influence of projectile impact velocity and target material on the process of projectile penetration

In this sub-chapter 3.3.1, an analysis of the influence of the variation in the impact velocity of the projectile on the exit velocity of the projectile was performed. The analysis was performed for the 0.2 mm mesh size (which was adopted earlier as the reference in the numerical model validation process) and the AA5083H116 target for different projectile impact velocities.

In the sub-chapter 3.3.2, the influence of the variation in the target material on the projectile penetration process was performed. The analysis was performed also for a mesh size of 0.2 mm and a projectile impact velocity of 822.4 m/s for different target materials.

# 3.3.1. The effect of changing the impact velocity of the projectile

In this part of the research, numerical simulations of the penetration of the 7.62mm x 63 projectile through the AA5083H116 target were carried out for different impact velocities of the projectile at a mesh size of 0.2 mm. The projectile and target materials, as well as the material models used, are the same as in the validation of the numerical model. The projectile and target geometry are also the same. For an impact velocity of 400 m/s, the projectile does not pass through the target.

The ballistic limit velocity is the input velocity at which the exit velocity obtained by numerical simulation is equal to 0. This ballistic limit velocity is obtained as the average velocity between the highest velocity of the projectile that does not penetrate the target and the lowest velocity of the projectile that completely passes through the target. In our case, the ballistic limit velocity was  $V_{bl} = 401$  m/s. After estimating the ballistic limit velocity, the calculation for the exit velocity of the projectile corresponding to the given input velocity was also carried out using the Recht–Ipson model. Output velocities were calculated based on the following empirical model originally proposed by Recht and Ipson [9]:

$$v_r = a \cdot (v_i^p - v_{bl}^p)^{\frac{1}{p}} \tag{8}$$

where:

 $v_i$  – impact velocity,  $v_r$  – exit velocity,  $v_{bl}$  – ballistic limit velocity, a and p – Recht constants of the model.

Regression analysis (of data obtained by simulations) was used to determine the parameters a and p from the Recht-Ipson model as accurately as possible. The determination of these parameters was performed using the "Matlab" program ("Curve Fitting Tool" option, the values of the projectile's impact and exit velocity obtained by simulation are used).

Figure 9 shows a graph of projectile exit velocity versus projectile impact velocity for numerical simulations and the Recht-Ipson model with obtained constants.

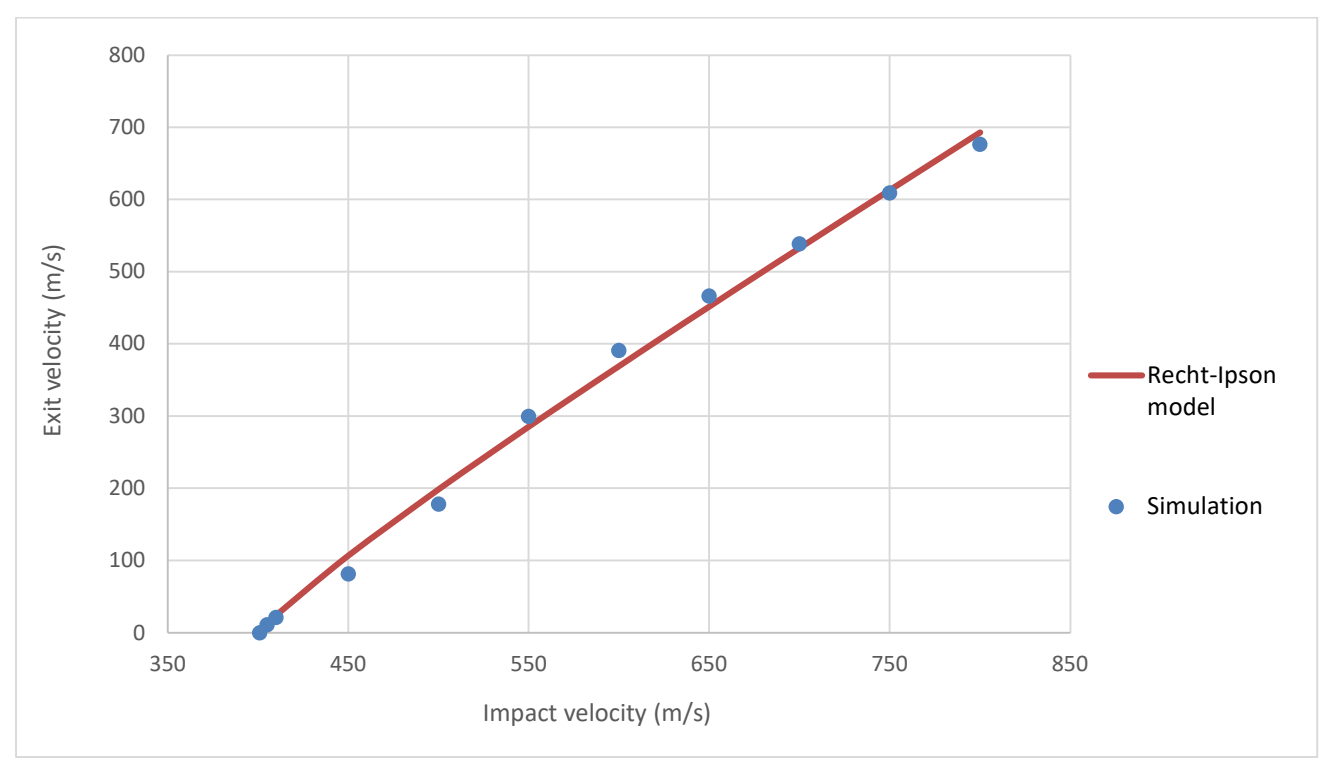


Figure 9. Diagram of exit velocity of the projectile as a function of projectile impact velocity (simulation results and Recht-Ipson curve)

By using the equation of the Recht-Ipson model curve whose constants are obtained by regression based on the results of the numerical simulation, the output velocity of the projectile can be determined for different values of the input velocity of the projectile without starting the simulation. This model is most often used for cases of projectile impact at a normal angle to a thin target. The disadvantage of this model is that in order to obtain the constants, experimental testing or numerical simulation must be carried out in order to obtain the constants by regression of the test/simulation results.

### 3.3.2. The effect of changing the target material

Numerical simulations in this part of the research were performed for the same conditions as in the previous chapters. The material of the projectile parts is also unchanged, the only variation is in the 20 mm thick target material. It is assumed that the equation of state for all steels is the same and the constants of this equation are listed in Table 4. Tables 5 and 6 lists the Johnson-Cook strength model constants and fracture model constants for various target materials.

Table 4. Coefficients of the Gruneisen shock equation of state for the target material [10]

Material	Density (g/cm <sup>3</sup> )	Gruniesen coefficient	$c_0$ (m/s)	S
Steel/iron	7,85	1,93	4570	1,49

Table 5. Johnson-Cook strength model constants for various target materials

Material	A (MPa)	B (MPa)	n	С	m
Steel 4340 [Autodyn library]	792	510	0,26	0,014	1,03
Armox 500T [11]	1372,4	835	0,2467	0,0617	0,84
Mild steel [11]	304,3	422	0,345	0,0156	0,87
RHA steel [12]	1193	500	0,676	0,00435	1,17
Weldox 460E steel [13]	490	807	0,73	0,012	0,94
Weldox 700E steel [14]	859	329	0,579	0,0115	1,071
Weldox 900E steel [4]	992	364	0,568	0,0087	1,131
Iron Armco [Autodyn library]	175	380	0,32	0,06	0,55
Bainite steel [15]	1517	1575	0,35	0,01	1
Nanos-BA steel [12]	1303	1420	0,195	0,075	1,17
Steel Tenax [16]	1440	492	0,24	0,011	1,03
Steel 2P [16]	1210	773	0,26	0,014	1,03

Table 6. Johnson-Cook failure model constants for different target materials

Material	$D_1$	$D_2$	$D_3$	$D_4$	$D_5$
Steel 4340 [Autodyn library]	0,05	3,44	-2,12	0,002	0,61
Armox 500T [11]	0,04289	2,1521	-2,7575	-0,0066	0,86
Mild steel [11]	0,1152	1,0116	-1,7684	-0,05279	0,5262
RHA steel [12]	0,21	7,2	-5,44	0	0
Weldox 460E steel [13]	0,0705	1,732	-0,54	-0,0123	0
Weldox 700E steel [14]	0,361	4,768	-5,107	-0,0013	1,333
Weldox 900E steel [14]	0,294	5,149	-5,583	0,0023	0,951
Iron Armco [Autodyn library]	-2,2	5,43	-0,47	0,016	0,63
Bainite steel [15]	0,047	0,165	-2,7	0	0
Nanos-BA steel [12]	0,047	0,165	-2,7	0	0
Steel Tenax [16]	0	1,07	-1,22	0,000016	0,63
Steel 2P [16]	0,1	0,93	-1,08	0,000014	0,65

Numerical simulation results, i.e. the penetration process of the 7.62mm x 63 projectile through targets made of different steels at a projectile impact velocity of 822.4 m/s and a mesh size of 0.2 mm are shown in Figure 10. The material of the target in the figure is given in the legend and is marked in blue.

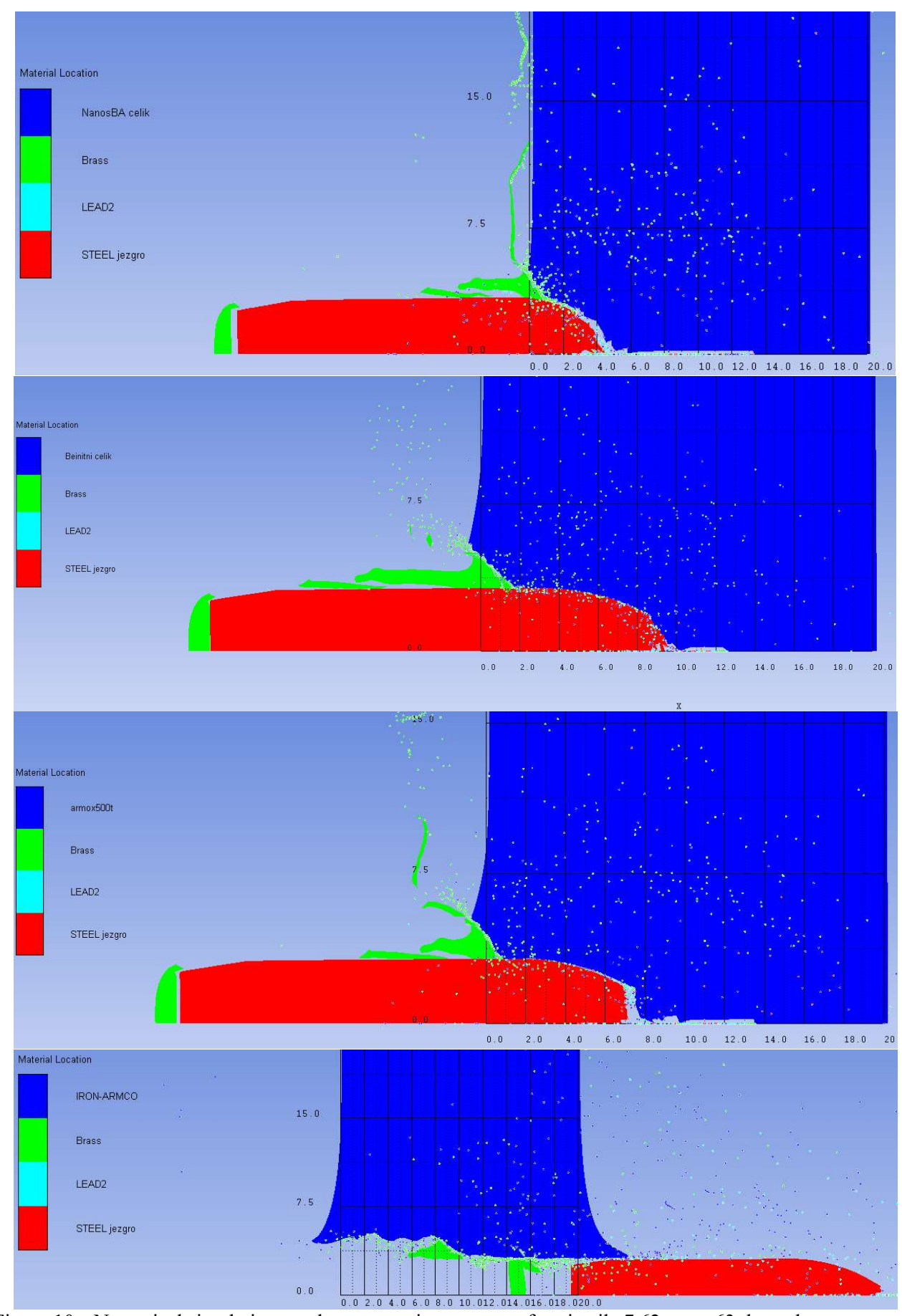


Figure 10a. Numerical simulation results: penetration process of projectile 7.62mm x 63 through targets made of different steels at projectile impact velocity 822.4 m/s and mesh size 0.2 mm

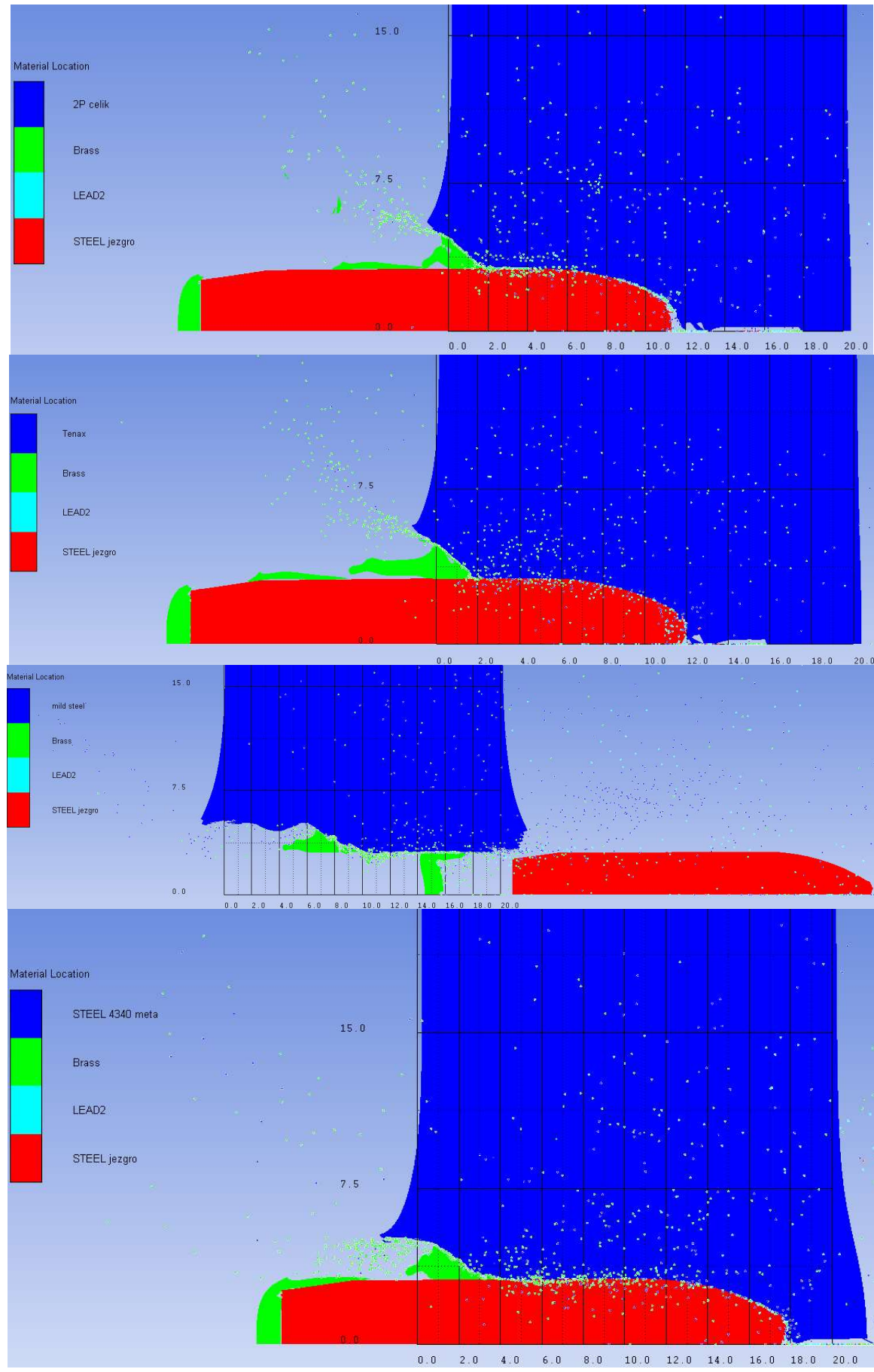


Figure 10b. Numerical simulation results: penetration process of projectile 7.62mm x 63 through targets made of different steels at projectile impact velocity 822.4 m/s and mesh size 0.2 mm – continued

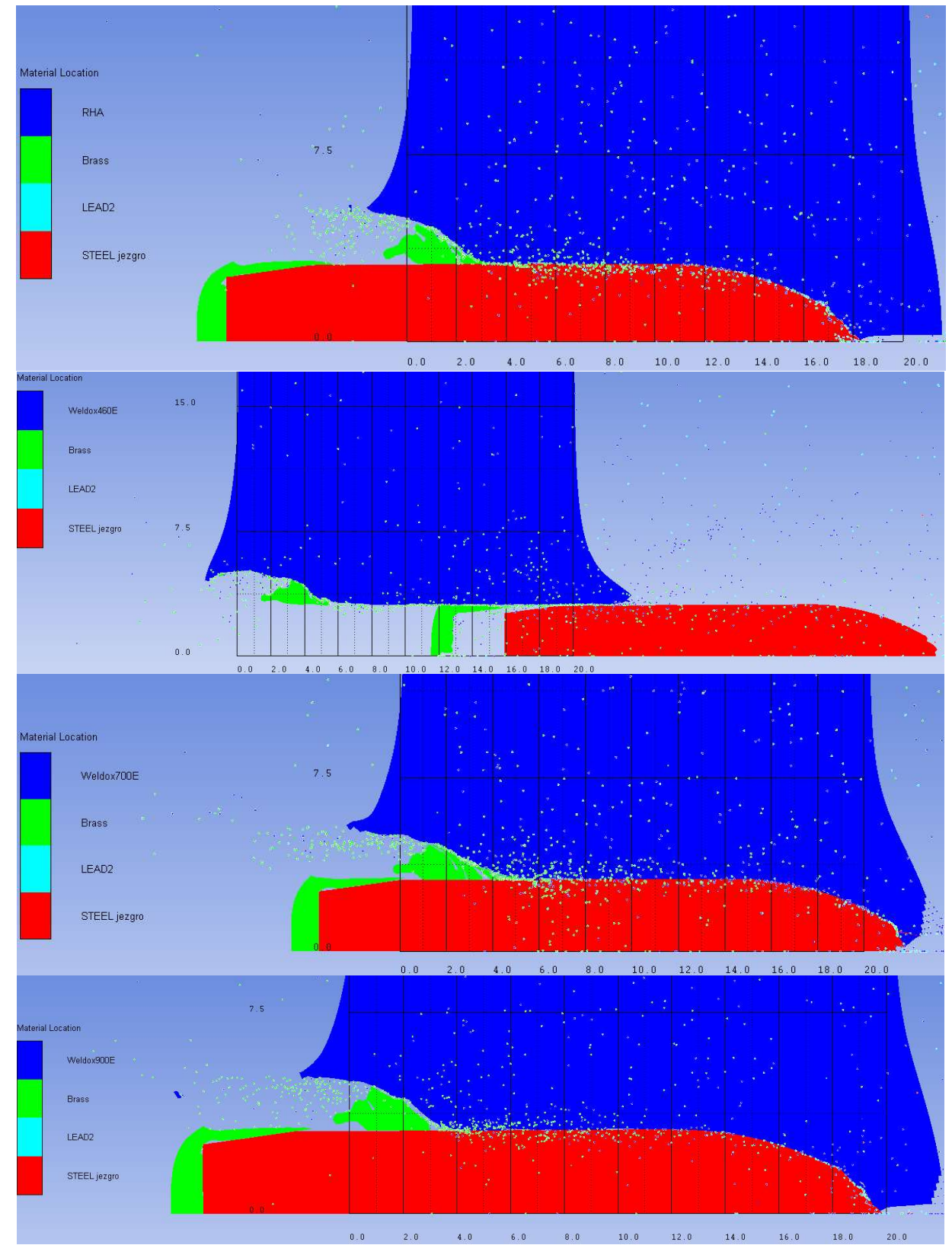


Figure 10c. Numerical simulation results: penetration process of projectile 7.62mm x 63 through targets made of different steels at projectile impact velocity 822.4 m/s and mesh size 0.2 mm – continued

Table 7 shows the penetration depths of the 7.62mm x 63 projectile through targets made of different steels at an impact velocity of 822.4 m/s. In Figures 10a-c and Table 7, it can be noted that the most durable steels are bainite steels (Nanos-BA steel and bainite) as well as Armox 500T steel.

The 2P and Tenax steels also showed relatively good performance against the 7.6 2mm x 63 projectile, retaining the projectile in the target after penetrating a little more than half the thickness of the target.

RHA and 4340 steels did not perform as well, where the 7.62 mm x 63 projectile penetrated almost the entire target, but remained stuck the target. They have shown better durability than the materials listed below.

Weldox 460E, Weldox 700E, Iron Armco, and mild steel showed lower effectiveness than the previous steels in penetration of the 7.62mm x 63 projectile at 822.4 m/s and the projectile completely penetrated targets with these materials. Mild steel showed the weakest performance as the projectile completely exited the target, while with the materials mentioned before (bainite steels, Armox 500T, 2P, 4340 and Tenax steels, RHA, Weldox 700E and Weldox 900E) the projectile remained stuck in the target.

Table 7. The penetration depth of the projectile 7.62 mm x 63 through a target made of different steels at a projectile impact velocity of 822.4 m/s

Target material	Penetration depth (mm)
Nanos-BA steel	4,5
Armox 500T	7,7
Bainite steel	9
Steel 2P	11
Steel Tenax	12
Steel 4340	18
RHA	18
Weldox 900E	19,5
Mild steel	20 (perforation)
Iron Armco	20 (perforation)
Weldox 460E	20 (perforation)
Weldox 700E	20

The data required for the analysis of the influence of mechanical characteristics on the penetration depth of the 7.62x63 mm projectile through the target are set out in Table 8.

The hardness of a material is a measure of the material's resistance to indentation, abrasion, and wear. For metals, the hardness of a material can be related to a material's UTS (ultimate tensile strength) with a linear relationship, which is shown in the diagram of tensile strength as a function of hardness (figure 11).

In the diagram in Figure 11, approximately mean values are used for parameters whose exact value is not known, but the range of values is known. It can be seen in Table 8 that a material with a higher hardness has a higher tensile strength. Increasing the hardness of steel leads to an increase in the ballistic protection of armor materials. High hardness contributes the most to the reduction of penetration depth. This is evident in materials such as Armox 500T and bainite steel, which have relatively small penetration depths. Materials with relatively high hardness (eg Weldox 900E) resist projectile penetration better than materials with lower hardness (eg Iron Armco). This can be seen from the fact that although the Weldox 900E and Weldox 700E steels have approximately the same penetration depth of 20 mm, the projectile in these cases failed to completely penetrate them, while it completely penetrated the softer Iron Armco and Weldox 460E steels.

	_	*	
Material	Hardness	Tensile strength	Penetration depth
Iviateriai	(BHN)	(MPa)	(mm)
Nanos-BA steel	590-640 [18]	1800-2000 [18]	4,5
Armox 500T	480-540 [10]	1450-1800 [10]	7,7
Bainite steel	373-627 [20]	1770-2200 [19]	9
Steel 4340	321 [21]	1100 [21]	18
RHA steel	302-400 [22]	1170 [23]	18
Mild steel	105 [24]	365 [24]	20 (perforation)
Iron Armco	74-83 [25]	290 [25]	20 (perforation)
Weldox 460E	171-181 [26]	530-720 [17]	20 (perforation)
Weldox 700E	210-240 [27]	780-930 [27]	20
Weldox 900E	280-330 [28]	940-1100 [29]	19,5

Table 8. Mechanical properties of the target material and penetration depth of the 7.62 mm x 63 projectile

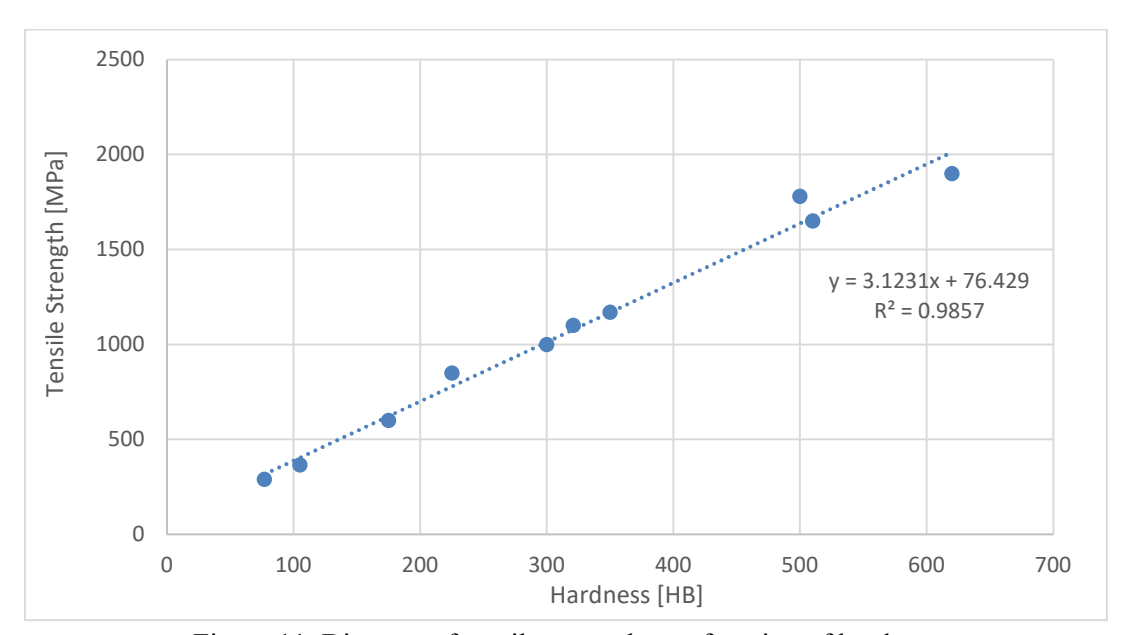


Figure 11. Diagram of tensile strength as a function of hardness

High strength and ductility are assumed to be vital parameters in order to absorb energy during structural impact [14]. Ductility is the ability of a material to withstand plastic deformation without breaking. The more a material is capable of withstanding greater deformation without brittle fracture, the more ductile the material is. For materials that are subjected to relatively high strain rates (when compared to quasi-static values), their strengths can change and, for most materials, increase markedly. Generally speaking, metals will get stronger but less ductile at elevated strain rates, but unlike some non-metals, their stiffness is relatively unaffected by increased deformation rates. The reason for the increased strength with strain rate is due to complex microstructural behavior that is dependent on the nature of the material (at high deformation rates, dislocations accumulate within the material structure and the material hardens) [17].

In addition to hardness and ductility, the mechanical properties to pay attention to are also yield strength, tensile strength, and toughness. The area under the curve on a Hooke diagram (stress diagram) is a measure of the strain energy absorbed per unit volume, V, and is an indication of the toughness of the material. For an armor designer, toughness is a desirable property because a tough material requires more energy to cause fracture. High tensile strength and yield strength allow steel to resist deformation and maintain structural integrity under high stress [17]. A material such as RHA steel, while not the hardest of the given steels, has a high tensile strength, which helps to better absorb and dissipate projectile energy.

It is noticeable that the steels with the highest resistance to projectile penetration are the steels with the highest hardness and tensile strength. Because of this, targets such as mild steel and Iron Armco suffer full penetration compared to bainitic steels and Armox 500T steel. The iron-Armco has 7-8 times lower hardness than Nanos-BA steel and 5 times lower tensile strength.

The diagram of penetration depth as a function of tensile strength in Figure 12 was obtained on the basis of data from Table 8, where approximately mean values were used for material properties whose exact value is not known, but the range of values is known. Looking at the plot of penetration depth as a function of tensile strength, it can be concluded that tensile strength is a good indicator of armor performance. It can be clearly seen that the penetration depth decreases with increasing tensile strength, with a small deviation for the Armox 500T steel.

The diagram of penetration depth as a function of hardness (Figure 13) was obtained in the same way as the diagram from Figure 12. On the diagram of the depth of penetration as a function of hardness, as well as on the diagram from Figure 12, it is seen that increasing the hardness decreases the depth of penetration. Similar results and conclusions about the influence of tensile strength and hardness are given in reference [30].

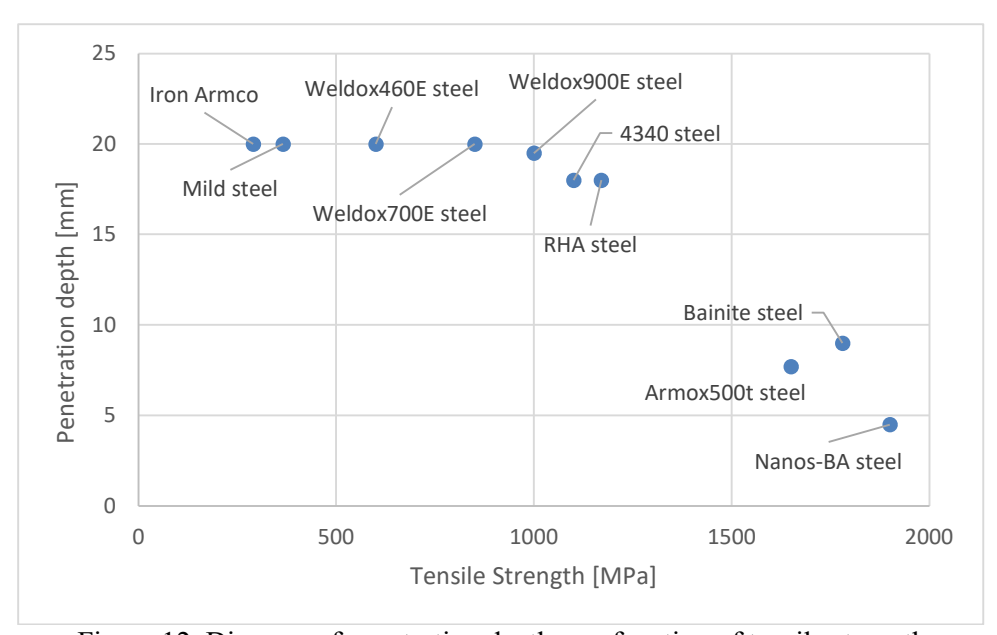


Figure 12. Diagram of penetration depth as a function of tensile strength

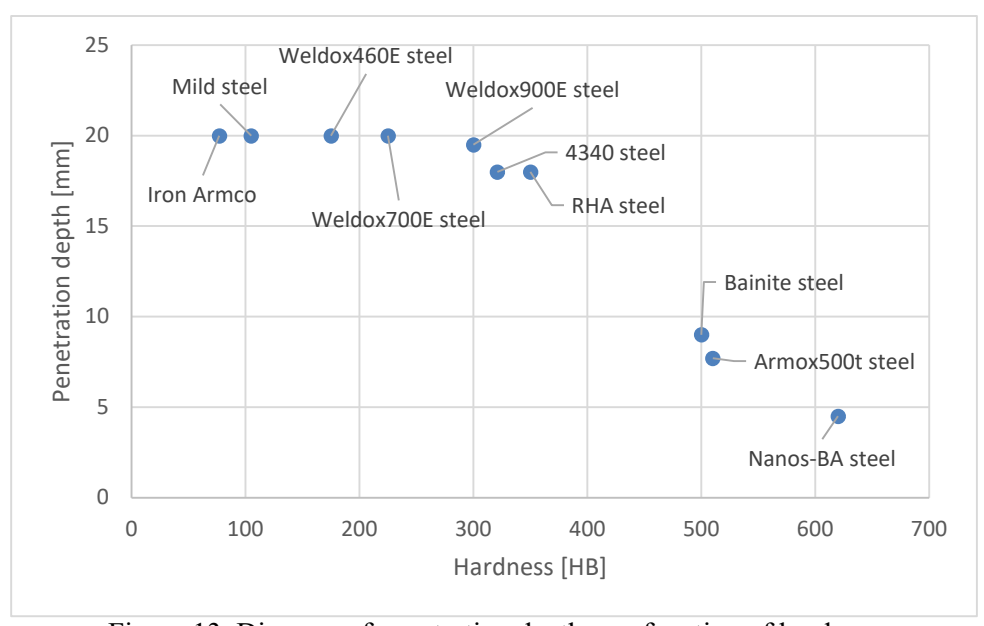


Figure 13. Diagram of penetration depth as a function of hardness

#### 4. Conclusions

The study evaluates the penetration capability of small-caliber projectiles using numerical simulation methods. Numerical simulations were performed using Ansys Autodyn software, simulating the penetration of a 7.62mm x 63, AP, M2 projectile through targets made of different materials. For model validation, reference [8] was used to confirm the model's validity, as the results of the projectile's exit velocity from the numerical

simulation closely matched the experimental results reported in the literature [8] (a relative error of 1.65% was obtained).

After validating the model, an analysis was conducted on the impact of varying the projectile's input velocity and changing the target material for the same input velocity. The projectile exit velocities obtained from numerical simulations showed good agreement with the exit velocities calculated using the Recht-Ipson model. It was also observed, as expected, that the reduction in the projectile's exit velocity as a function of impact velocity is nearly linear. The projectile's exit velocity can be determined for different input velocities without running additional simulations by using the Recht-Ipson model.

Material hardness is a measure of a material's resistance to indentation, abrasion, and wear, and can be correlated with its maximum tensile strength through a linear relationship. It is assumed that high strength and ductility are key parameters for the target material's ability to absorb energy upon impact. For armor designers, toughness is also a desirable property, as a tough material requires more energy to fracture. The analysis of changing the target material for the same input projectile velocity (822.4 m/s) showed that bainitic steels (with the highest hardness) were the most resilient, followed by Armox 500T steel. Examining the effect of changing the target material for the same input projectile velocity, it can be concluded that ballistic protection can be increased by increasing the material's hardness and tensile strength, with a clear reduction in penetration depth as the hardness and tensile strength of the target material increase.

For future work, further research is recommended to expand the analysis of the influence of various factors on projectile penetration. Special attention should be paid to variations in projectile and target geometry, as well as the possibilities for optimizing materials to increase resistance to penetration. Additionally, research should encompass a wider range of calibers and types of projectiles to gain a more comprehensive understanding of penetration dynamics in different situations. The study could be expanded by using multi-layer targets and varying target thickness, allowing for the measurement of maximum projectile penetration depths. Investing in computer equipment would enable the performance of 3D numerical simulations, facilitating high-quality testing of projectile impacts on angled targets set at specific angles relative to the direction of fire. Investing in computer equipment could also save money compared to the costs required for conducting experimental tests. In experimental studies, systems such as high-speed cameras could be implemented where feasible.

#### **Funding information**

No funding was received from any financial organization to conduct this research.

# **Declaration of competing interest**

The authors declare that they have no known competing financial interests or personal relationships that could have appeared to influence the work reported in this paper.

#### References

- [1] https://modernfirearms.net/en/cartridge/30-06-us-306-7-62x63mm-30-cal-1906/
- [2] NIJ Standard-0101.06:200 Ballistic Resistance of Body Armor, U.S. Department of Justice Office of Justice Programs, Washington, USA.
- [3] Army Ammunition Data Sheets Small Caliber Ammunition FSC 1305 TM-43-0001-27 Headquarters, Department of the Army, April 1994.
- [4] https://www.goofygoatgifts.com/product-page/30-06-bullet-pendant
- [5] A. Ćatović, Numerical simulations in ballistics, Mechanical Engineering Faculty, Sarajevo, 2024.
- [6] AUTODYN® Explicit Software for Nonlinear Dynamics, Theory Manual Revision 4.3., 2005.
- [7] G. Ozturk, "Numerical and experimental investigation of perforation of ST-37 steel plates by oblique impact [MS thesis]", The graduate of School of Natural and Applied Sciences of Middle East Technical University, 2010.
- [8] T. Borvik, L. Olovsson, S. Dey, M. Langseth, "Normal and oblique impact of small arms bullets on AA6082-T4 aluminum protective plates", *International Journal of Impact Engineering*, vol 38, pp. 577-589, 2011.

- [9] M. A. Iqbal, K. Senthil, P. Bhargava, N. K. Gupta, "The characterization and ballistic evaluation of mild steel", *International Journal of Impact Engineering*, vol. 78, pp. 98-113, 2015.
- [10] A. Mubashar, E. Uddin, N. Arif, S. W. Ul Haq, M. Chowdhury, "Ballistic response of 12.7 mm armour piercing projectile against perforated armour developed from structural steel", *Proceedings of the Institution of Mechanical Engineers, Part L: Journal of Materials: Design and Applications*, vol. 233, Issue 10, October 2018.
- [11] K. Senthil, M. A. Iqbal, S. Rupali, "Influence of impactor nature, mass, size and shape on ballistic resistance of mild steel and Armox 500 T steel", *International Journal of Protective Structures*, pp. 1-24, 2018.
- [12] T. Fras, A. Murzyn, P. Pawlowski, "Defeat mechanisms provided by slotted add-on bainitic plates against small-calibre 7,62x51 AP projectiles", *International Journal of Impact Engineering*, vol. 103, pp. 241-253, 2017.
- [13] T. Borvik, M. Langseth, O. S. Hopperrstad, K. A. Malo, "Ballistic Penetration of Steel Plates", *International Journal of Impact Engineering*, vol. 22, No. 9-10, pp. 855-886, 1999.
- [14] S. Dey, T. Borvik, M. Langseth, O. S. Hopperrstad, J. R. Leinum, "The effect of target strength on the perforation of steel plates using three different projectile nose shapes", *International Journal of Impact Engineering*, vol. 30, No. 8-9, pp. 1005-1038, 2004.
- [15] W. Burian, P. Zochowski, M. Gmitrzuk, J. Marcisz, L. Starczewski, B. Juszczyk, M. Magier, "Protection effectiveness of perforated plates made of high strength steel", *International Journal of Impact Engineering*, 2018.
- [16] J. Buchar, J. Voldrich, S. Rolc, J. Lisy, "Ballistic performance of the dual hardness armour", *Proceedings of 20th International Symposium on Ballistics*, Orlando, pp. 23-27, 2020.
- [17] P. Hazell, Armour Materials, Theory and Design, Second Edition, CRC Press, 2023.
- [18] B. Garbarz, W. Burian, J. Marcisz, A. Wisniewski, "The Nano-Duplex NANOS-BA Steel for Application in Construction of Armours", *Problems of mechatronics, Armament, Aviation, Safety Engineering*, vol. 4, No. 10, pp. 7-22, ISSN 2081-5891, 2012.
- [19] C. M. Garcia, F. G. Caballero, H. K. D. H. Bhadeshia, "Mechanical properties of low-temperature bainite", *Materials Science Forum*, vol 500, pp. 495-502, 2005.
- [20] https://www.totalmateria.com/en-us/articles/bainite-hardening-of-steel-1
- [21] https://www.techsteel.net/alloy/steel/4340
- [22] https://www.chapelsteel.com/mil-a-12560.html
- [23] https://home.agh.edu.pl/~jrichert/Tablica Ti.htm
- [24] https://www.xometry.com/resources/materials/mild-steel/
- [25] https://www.aksteel.nl/files/downloads/172888 armco pure iron pdb euro final secured 92.pdf
- [26] P. A. Prabowo, I. Haryanto, "Analisa keceptan sisa proyektil berhidung tumpul yang ditembakkan pada baja Weldox 460 E", *Jurnal Tehnik Mesin S-1*, vol. 2, No. 1, Tahun, 2014.
- [27] https://blog.thepipingmart.com/grades/weldox-700e-composition-properties-and-uses/
- [28] Weldox 900: High-Strength Structural Steel Plate, Alloy Digest, ASM International, vol. 56, 2007.
- [29] Weldox 900 Datasheet, SSAB Oxelösund AB, Version 2005-10-15
- [30] K. L. Phelps, "Material properties affecting the penetration of metal targets by copper linear shaped charges [MS thesis]", Missouri University of Science and Technology, 2016.
- [31] A. Catovic, "Research of influence of different shaped charge liner materials on penetration depth using numerical simulations", *Periodicals of Engineering and Natural Sciences*, vol 11, No. 4, pp. 1-26, 2023.
- [32] A. Catovic, "Estimation of terminal ballistics parameters for several 7.62×51 mm projectiles using numerical simulations", *The Journal of Defense Modeling and Simulation: Applications, Methodology, Technology*, 2024.